Infrared Photodissociation Spectroscopy of $Al^+(CH_3OH)_n$ (n=1-4)

Ari Furuya[1], Mamoru Tsuruta[1], Fuminori Misaizu[*1], Koichi Ohno[1], Yoshiya Inokuchi[2,3], Ken Judai[2], and Nobuyuki Nishi[*2]

[1]*Department of Chemistry, Graduate School of Science, Tohoku University, Aramaki, Aoba-ku, Sendai 980-8578, Japan*

[2]*Institute for Molecular Science, Nishigo-naka 38, Myodaiji, Okazaki 444-8585, Japan*

[3]*Department of Chemistry, Graduate School of Science, Hiroshima University, Higashi-Hiroshima 739-8526, Japan*

Received ;

Abstract

Infrared photodissociation spectra of $Al^+(CH_3OH)_n$ (n=1-4) and $Al^+(CH_3OH)_n$-Ar (n=1-3) were measured in the OH stretching vibration region, 3000-3800 cm^{-1}. For n=1 and 2, sharp absorption bands were observed in the free OH stretching region, all of which were well reproduced by the spectra calculated for the solvated type geometry with no hydrogen bond. On the other hand, for n=3 and 4, there were broad vibrational bands in the energy region of hydrogen bonded OH stretching vibrations, 3000-3500 cm^{-1}. Energies of possible isomers for the $Al^+(CH_3OH)_{3,4}$ ions with hydrogen bonds were calculated in order to assign these bands. It is found that the third and fourth methanol molecules form hydrogen bonds with methanol molecules in the first solvation shell, rather than a direct bonding with the Al^+ ion. We obtained no evidence of the insertion reaction for the present $Al^+(CH_3OH)_n$ system, which was reported in $Al^+(H_2O)_n$ previously. One possible explanation of the difference between these two systems is that the potential energy barriers between the solvated and inserted

[*] To whom correspondence should be addressed. E-mail: misaizu@qpcrkk.chem.tohoku.ac.jp

isomers in the $Al^+(CH_3OH)_n$ system is too high to form the inserted type isomers.

1. Introduction

Gas phase clusters have long been the subject of interest, because it can be regarded as microscopic models of condensed phase, and also because there may still remain unveiled novel species in this phase. However, it was difficult to obtain detailed information on structures of the clusters until recently except for some specific systems. This difficulty is caused by the relatively low concentration of the clusters, which makes the application of usual spectroscopic techniques impossible. Recently, photodissociation spectroscopy using infrared (IR) light has been widely applied in order to investigate structures of cluster ions such as molecular cluster ions,[1-5] metal cluster ions,[6] and metal-molecule binary cluster ions[7-9] because of the development of strong IR light sources. In particular, cluster ions including water molecules such as protonated water clusters, $H^+(H_2O)_n$, and hydroxide ion-water clusters, $OH^-(H_2O)_n$, have been extensively studied as microscopic models of condensed phase because of their fundamental importance in the biochemistry, aqueous chemistry, and so on.[1-5] On the other hand, binary clusters consisting of a metal atom (or its ion) and some polar molecules have been also examined for a large number of systems in order to elucidate solvation structures in the clusters.[7-9] Along with the stepwise solvation structures, intracluster reactions were also reported in the metal-molecule binary clusters such as intracluster cyclization reaction in a Ni^+-C_2H_2 system.[10] More recently, Inokuchi et al. reported the results on IR photodissociation spectroscopy of cluster ions including aluminum monocation and water molecules, $Al^+(H_2O)_n$ (n=1 and 2), in which an insertion reaction of Al^+ into an OH bond of a water molecule was found to occur in $Al^+(H_2O)_n$.[11] This insertion reaction proceeds in the cluster size of n=2 whereas a solvated type isomer having a direct bond between Al^+ and an O atom of water, Al^+-OH_2, was formed at n=1. For the n=1 ion,

the OH-inserted isomer was reported to be a metastable structure, which was 49.36 kJ/mol higher in energy than the solvated type isomer.[12] On the other hand, the inserted type isomer was calculated to be more stable than the solvated type isomer for n=2. Thus the experimentally observed isomers in $Al^+(H_2O)_n$ were explained by their relative stability. The insertion reaction of Al^+ ion into an NH bond of an NH_3 molecule were also reported in $Al^+(NH_3)_n$, which can be explained by their energetics again.[13] On the basis of these recent examinations, it is highly interesting to examine whether the Al^+ ion can insert into CO or OH bonds of methanol molecule or not. In this study, geometrical structures and a possibility of insertion reactions in the cluster ions with an aluminum monocation and methanol molecules, $Al^+(CH_3OH)_n$, have been studied by using IR photodissociation spectroscopy along with theoretical calculation.

2. Experiment

Details of the experimental setup have been described elsewhere.[11] The apparatus consists of an ion-guide mass spectrometer with two quadrupole mass filters. Cluster ions containing aluminum monocation, Al^+, and methanol molecules, CH_3OH, were produced in a pickup source with a combination of laser vaporization and supersonic expansion. A rotating and translating Al rod (6 mm diameter), which was mounted 10 mm downstream from a pulse valve (General Valve, Series 9, orifice diameter 0.8 mm), was irradiated with the second harmonic of a Nd:YAG laser (Spectra Physics, INDI-50) to produce the Al^+ ion. Synchronized with the generation of the Al^+ ion, methanol vapor seeded in argon buffer gas was expanded from the pulse valve to form methanol clusters. The mixture gas of methanol and argon was obtained by passing Ar gas through a reservoir containing liquid methanol. A mixing ratio was determined by optimizing the ion intensity of a given size. Cluster ions containing Al^+ and CH_3OH were then produced by collisions between the metal ion and the

molecular clusters. After the collimation with a conical skimmer, the produced ion beam was introduced into the first quadrupole mass filter with a 50 eV kinetic energy.

After the mass isolation of the parent cluster ions with the first quadrupole mass filter, the selected ions were deflected at a right angle in the ion bender, and they were introduced into the quadrupole ion guide operated in RF-only mode. These parent ions were then irradiated with a counterpropagating infrared light, which induced vibrational excitation of the ions when a frequency of the light matched with a vibrational frequency. Vibrational excitation of the parent ions results in a fragmentation of the ions after the intra- and intermolecular vibrational energy relaxation. Resultant fragment ions were mass-analyzed by the second quadrupole mass filter and detected by a secondary electron multiplier tube. Ion signals from the detector were stored in a digital storage oscilloscope (LeCroy, 9314A) and were typically averaged over 200 laser shots.

An optical parametric oscillator (OPO) system (Continuum, Mirage 3000) pumped by an injection-seeded Nd:YAG laser (Continuum, Powerlite 9010) was used as a tunable infrared light source. The output energy and the linewidth are typically 1-2 mJ/pulse and ~1 cm^{-1}, respectively. In order to prevent saturation and nonresonant multiphoton processes, the infrared light was loosely focused before entering the vacuum chamber. Energy of the obtained infrared light was calibrated by a commercial wavemeter (Burleigh, WA-4500). Photofragment ion yield was normalized by the intensity of the infrared light and also by the parent ion signal, to minimize fluctuations with time and to improve signal-to-noise ratio of the dissociation spectra. Photodissociation spectra were obtained by plotting fragment ion intensity as a function of photon energy.

A messenger technique with an Ar atom is used to form cold cluster ions and also to enhance the dissociation probability after photon absorption because the binding energy of Ar atom is comparatively small. For example, bond dissociation energy of Al^+-Ar in the ground

state was determined to be 1025 cm^{-1},[14] which is much smaller than the energy of OH stretching vibration (3000-3800 cm^{-1}). Thus, the dissociation of the Ar atom from $Al^+(CH_3OH)_n$-Ar to produce bare $Al^+(CH_3OH)_n$ was easily caused by the absorption of an infrared photon corresponding to OH stretching vibration. Therefore, we can obtain enhanced signals from a parent ion of $Al^+(CH_3OH)_n$-Ar with small internal energy.

3. Calculation

Geometrical structures of $Al^+(CH_3OH)_n$ (n=1-4) and $Al^+(CH_3OH)_n$-Ar (n=1-3) cluster ions were optimized by a density functional theory (DFT) calculation with Becke-3-Lee-Yang-Parr (B3LYP) functional[15] of the Gaussian 03 package.[16] Harmonic vibrational frequencies were also calculated at the same level of theory in order to ensure that equilibrium structures were obtained in the geometry optimization. Energies of the calculated geometries are corrected by zero-point vibrational energy by using the harmonic frequencies. Theoretical vibrational spectra were obtained by the calculated frequencies and IR intensities with a frequency-scaling factor of 0.9654.

4. Results

Infrared photodissociation spectra of $Al^+(CH_3OH)_n$ (n=1-4) are shown in Fig. 1 (broken lines), which were obtained by monitoring $Al^+(CH_3OH)_{n-1}$–ion yields formed by a loss of a methanol molecule. In Figs. 1(a) and 1(b), relatively broad bands were observed in the spectra, peaking at 3485 cm^{-1} with full width at half maximum (FWHM) of 130 cm^{-1} for $Al^+(CH_3OH)_1$ and 3579 cm^{-1} with FWHM of 90 cm^{-1} for $Al^+(CH_3OH)_2$ clusters. On the other hand in Figs. 1(c) and 1(d), quite broad bands with more than 200 cm^{-1} FWHM were observed in the region under 3500 cm^{-1} as well as sharp absorption bands (FWHM ~ 50 cm^{-1}) above 3500 cm^{-1} for $Al^+(CH_3OH)_3$ and $Al^+(CH_3OH)_4$ ions. In the spectrum of $Al^+(CH_3OH)_3$,

two discernible vibrational bands appeared at 3594 and 3654 cm^{-1} whereas broad bands were observed in the region of 3000-3500 cm^{-1}. For $Al^+(CH_3OH)_4$, a sharp band peaking at 3663 cm^{-1} and at least two broad bands in <3200 and 3000-3500 cm^{-1} were observed in the spectrum. Observed frequencies are summarized in Table 1.

Solid lines in Fig. 1 show infrared photodissociation spectra of Ar-attached $Al^+(CH_3OH)_n$ (n=1-3) clusters. Observed band widths in these spectra were considerably narrower than those of bare $Al^+(CH_3OH)_n$ due to the reduced internal energies in the Ar-attached cluster ions. In the infrared spectrum of $Al^+(CH_3OH)_1$-Ar, a sharp vibrational band was observed at 3495 cm^{-1} in addition to a very weak band around 3550 cm^{-1}. For $Al^+(CH_3OH)_2$-Ar ion, two distinct vibrational bands were observed at 3567 and 3593 cm^{-1} in the spectrum. In the spectrum of $Al^+(CH_3OH)_3$-Ar, one can find the two strong vibrational bands at ~3300 and ~3370 cm^{-1} as well as the two sharp peaks at 3615 and 3630 cm^{-1}. Observed frequencies of $Al^+(CH_3OH)_n$-Ar (n=1-3) are also summarized in Table 1.

5. Discussion: Theoretical calculation and assignment of the cluster structures

A. $Al^+(CH_3OH)_1$ and $Al^+(CH_3OH)_1$-Ar

In order to get information on the geometries of $Al^+(CH_3OH)_1$ and $Al^+(CH_3OH)_1$-Ar ions, theoretical calculations of these ions were performed at B3LYP/6-31+G(d) level of theory.[15] Optimized structures of $Al^+(CH_3OH)_1$ are shown in Fig. 2(a). There are three isomers for $Al^+(CH_3OH)_1$ as shown in the figure; solvated (**1-I**, C_s symmetry), OH-inserted (**1-II**, C_{3v} symmetry), and CO-inserted (**1-III**, C_{3v} symmetry) types. The solvated type isomer, **1-I**, has a geometry where an Al^+ ion coordinates with a methanol molecule from the oxygen-atom side, whereas OH-inserted and CO-inserted types have geometries in which Al^+ inserts into OH and CO bonds of the methanol molecule, respectively. Among these, CO-inserted type, **1-III**, was calculated to be the most stable isomer. The energy of each

isomer relative to the most stable **1-III** isomer, ΔE_{rel}, is also shown in the figure.

Geometries of Ar attached ions, $Al^+(CH_3OH)_1$-Ar, were also calculated at the same level of theory. Binding sites of Ar atom at each isomer are shown by arrows in the figure. For **1-I**, there are two Ar-atom binding sites; one is the Al^+ ion and another is a hydrogen atom of the OH group of methanol. For the Ar attached ions, a lower-case letter is added to the notations of the bare $Al^+(CH_3OH)_1$ ion to distinguish the binding sites of Ar atom. The Ar atom in isomer **1-Ia** is located next to the Al^+ ion from the other side of the methanol molecule, whereas isomer **1-Ib** has a geometry in which the Ar atom binds with the hydrogen atom from the collinear direction with the O-H axis. For **1-II**, only an isomer **1-IIa** was calculated to be an equilibrium structure, where the Ar atom coordinates with the Al^+ ion at almost perpendicular direction to the molecular axis. Isomer **1-III** was found to have two Ar-atom binding sites as well as isomer **1-I**; isomers **1-IIIa** and **1-IIIb**. The former is the same kind of isomer **1-IIa**, that is, the Ar atom coordinates with the Al^+ ion from a perpendicular direction to the molecular axis. The latter has a geometry in which the Ar atom binds to an H atom of OH group from collinear direction with the O-H axis like **1-Ib**. The binding energy of the Ar atom was found to be lager for **1-Ib** (38 meV) than that for **1-Ia** (2 meV). This result is inconsistent with the simple consideration of an electrostatic interaction; charge – charge-induced dipole interaction between $Al^+(CH_3OH)_1$ and Ar. Natural charges on the Al atom and H atom of the OH functional group in **1-I** were calculated to be +0.96 and +0.57, respectively, as shown in Fig. 2(a). Thus, the electrostatic interaction in **1-Ia** is expected to be larger than that in **1-Ib**, if the charge – charge-induced dipole distance is the same. However, the calculated binding energy of the Ar atom showed opposite behavior as mentioned above. This can be explained by a repulsion between 3s electrons of the Al^+ ion and electron cloud of the Ar atom. In **1-I**, the highest occupied molecular orbital (HOMO) consists of the 3s orbital of Al, in which electron density of the

HOMO is localized on the Al atom especially at the opposite side of the methanol molecule as shown in Fig. 3. Therefore, the electron distribution in HOMO spreads over the region where the Ar atom approaches in **1-Ia**. The interaction between the positive charge of the Al^+ ion and charge-induced dipole moment of the Ar atom was thus compensated by the repulsion between the electrons of the HOMO and the electron cloud of the Ar atom. In a system composed of an alkali metal cation, M^+ (M=Na, K, Cs), and water, in which the cation has no *n*s electron, it was reported that the Ar atom coordinates with M^+ to form Ar-M^+-O configuration in $M^+(H_2O)$-Ar ions.[17] By contrast, Ar can be located on an H atom as well as an Mg^+ ion in the $Mg^+(H_2O)$-Ar, in which the metal cation has one 3s electron.[18] These previous results are consistent with the present calculation of the complex geometries.

The harmonic vibrational frequencies of both $Al^+(CH_3OH)_1$ and $Al^+(CH_3OH)_1$-Ar ions were also calculated at B3LYP/6-31+G(d) level in order to assign observed bands in the infrared photodissociation spectra and to determine geometries of these ions. Calculated vibrational spectra and vibrational frequencies are shown in Fig. 4 and Table 2, respectively. Here, the inserted-type isomers may not be probed at the present experimental condition because the Al^+ ion produced by the loss of a methanol molecule was monitored for the bare $Al^+(CH_3OH)_1$ ion. The Al^+ ion can be produced by the three body dissociation of isomers **1-II** and **1-III**, **1-II** $\rightarrow Al^+ + CH_3O + H$ and **1-III** $\rightarrow Al^+ + CH_3 + OH$. However, these fragmentation pathways are energetically impossible even if the inserted-type isomers are produced in the cluster beam at the present experimental condition. By contrast, signals from the inserted-type isomers can also be detected for the case of $Al^+(CH_3OH)_1$-Ar because the loss of the Ar atom is monitored in the present measurement. Thus, we focus our attention on the results of the $Al^+(CH_3OH)_1$-Ar ion in the rest part of this section. In Fig. 4, calculated vibrational spectrum of **1-Ib** was found to well reproduce the experimental spectrum of the $Al^+(CH_3OH)_1$-Ar ion. Furthermore, an OH stretching vibration of **1-Ia**

corresponds to the band observed at around 3550 cm^{-1} in the spectrum. Calculated vibrational spectra of isomers **1-IIa**, **1-IIIa**, and **1-IIIb** hardly correspond to the observed one. For example, **1-IIa** has no apparent peak around 3500 cm^{-1} because it has no OH functional group; the calculated peaks at 3068 and 3071 cm^{-1} for **1-IIa** correspond to CH stretching vibrations. By contrast, **1-IIIa** and **1-IIIb** show distinct peaks at 3767 and 3693 cm^{-1}, respectively. Thus, we attribute the predominant species in the cluster beam not to the most stable isomer **1-III** but to the solvated type isomer **1-I**. More detailed discussion on this insertion reaction is described below.

B. $Al^+(CH_3OH)_n$ (n=2-4) and $Al^+(CH_3OH)_n$-Ar (n=2, 3)

Fig. 2(b) shows optimized geometries of $Al^+(CH_3OH)_2$ calculated at the same level of theory as the $Al^+(CH_3OH)_1$ ions. There are at least three isomers of $Al^+(CH_3OH)_2$ as well as $Al^+(CH_3OH)_1$, solvated (**2-I**, C_2 symmetry), OH-inserted (**2-II**, C_1 symmetry), and CO-inserted (**2-III**, C_1 symmetry) types. These isomers have geometries in which the second methanol molecule coordinates with the each isomer of $Al^+(CH_3OH)_1$, **1-I** – **1-III**. For example, the second methanol molecule binds with the Al^+ ion of **1-I** from the same side of the first methanol with a bond angle of ∠O-Al^+-O=81° in the solvated type isomer **2-I**. An additional methanol also coordinates with the Al^+ ion of **1-II** and **1-III** in **2-II** and **2-III**, respectively. Among these, the most stable structure is the CO-inserted type isomer, **2-III**. The Ar-atom binding site, indicated by arrows in the figure, is the Al^+ ion or the H atoms of OH groups as already shown in the $Al^+(CH_3OH)_1$ ions. We discuss the structure of the $Al^+(CH_3OH)_2$ ion using the results on the Ar-attached ion as well as the n=1 ion. Calculated vibrational frequencies are summarized in Table 2. Vibrational spectra of the most stable structures in each type of isomers for the $Al^+(CH_3OH)_2$-Ar ion are also shown in Fig. 5 along with the experimentally obtained spectra. Only a spectrum of **2-Ib** can reproduce the

experimental spectrum of $Al^+(CH_3OH)_2$-Ar, having sharp doublet peaks in the region of free OH stretching vibrations. Therefore, **2-Ib** is an only species that can contribute to the dissociation spectrum predominantly. Although **2-III** has a characteristic vibration at the energy higher than 3700 cm^{-1}, no peaks were observed in this region of the experimental spectra [Fig. 5(a)]. Therefore, we concluded that **2-III** was not produced in the beam although it is the most stable among three isomers. For **2-II**, it has only one OH bond because the Al^+ ion inserts into an OH bond of the two methanol molecules. The vibrational frequency of the OH stretching mode of **2-IIb** was calculated to be slightly lower than the observed values. Therefore, **2-II** is less likely to be formed in the beam as well as **2-III**. The discussion on the insertion reactions will be presented in the next section.

Optimized geometries and calculated vibrational spectra of $Al^+(CH_3OH)_3$ are shown in Figs. 6 and 7, respectively. Seven isomers were obtained as equilibrium structures for the ion. Among these, two isomers, **3-I(3+0)** and **3-I(2+1)**, are classified as solvated type isomers whereas remaining five isomers are inserted types; **3-II(3+0)** and **3-II(2+1)** are OH-inserted and **3-III(3+0)**, **3-III(2+1)**, and **3-III(2+1)'** are CO-inserted type structures. Arabic numbers in the parentheses of the notation indicate the numbers of methanol molecules coordinating with the Al^+ ion directly (the first number) and those solvating to the other methanol molecules (the second number). For example, all methanol molecules directly solvate to the Al^+ ion in **3-I(3+0)**, whereas the third methanol binds with other methanol molecules by two hydrogen bonds in **3-I(2+1)**. The latter isomer has a geometry in which an additional methanol forms two hydrogen bonds with the H atoms of the OH functional groups in **2-I**, forming a six-membered ring. For the OH-inserted type isomers, the third methanol coordinates with the Al^+ ion of **2-II** in **3-II(3+0)**, and it binds with the H atom of the OH group of **2-II** in **3-II(2+1)**. In **3-III(3+0)**, the third methanol molecule binds with the Al^+ ion of the CO-inserted type **2-III**, whereas the third methanol coordinates with

the H atoms of the OH groups of **2-III** in **3-III(2+1)** and **3-III(2+1)'**. Among these seven isomers, **3-III(3+0)** was calculated to be the most stable, and energies of above isomers relative to **3-III(3+0)**, ΔE_{rel}, are also shown in Fig. 6.

The results of the bare $Al^+(CH_3OH)_3$ ion are discussed here in detail, before we turn to the Ar-attached ion for n=3. From the comparison of the experimental spectra with the calculated ones, **3-I(2+1)** [Fig. 6(c)] was found to reproduce the observed band feature. The calculated spectrum of **3-III(2+1)'** is also partly in agreement with the observed spectrum, especially for the free OH stretching region (above 3500 cm^{-1}), although the hydrogen bonded OH stretching of **3-III(2+1)'** (3183 cm^{-1}) was calculated to be lower than the observed band. However, **3-III(2+1)'** is the most unstable isomer among the CO-inserted type structures. It is unlikely that only the most unstable **3-III(2+1)'** is produced in the cluster beam even though the insertion reaction into the CO bond occurs. Thus, the most probable candidate is **3-I(2+1)**. In the free OH stretching region, however, the double peaks observed in the spectrum for bare $Al^+(CH_3OH)_3$ cannot be explained only by **3-I(2+1)**, because this isomer has one absorption band in this region. In the present laser vaporization source, there is a possibility that several different isomers including metastable ones are formed because of a hot condition in the source region. Other possible isomers, which may contribute to the spectrum having free OH stretching at ~3600 cm^{-1}, are **3-I(3+0)**, **3-II(3+0)**, and **3-II(2+1)** [Figs. 7(b), 7(d), and 7(e)]. Although the solvated-type isomer is less stable than the inserted-types, it is probable that **3-I(3+0)** is formed in the cluster beam as well as the n=1 and 2 ions. If the OH-inserted type isomers are formed as CH_3O-Al-$H^+(CH_3OH)_2$ ion, the most stable CO-inserted types may also be produced in the beam. However, no signals are observed at above 3700 cm^{-1} where the CO-inserted type isomers should show the bands characteristic to the OH group bound to Al^+. Therefore, the obtained spectrum of the $Al^+(CH_3OH)_3$ ion may have a contribution of **3-I(3+0)**.

Now, let us discuss the result of the Ar-attached ion of **3-I(2+1)**, which is the most probable candidate for the bare $Al^+(CH_3OH)_3$ structure. For the spectrum of the $Al^+(CH_3OH)_3$-Ar ion, signals from cold cluster ions contribute to the observed spectra predominantly because of the small binding energy of the Ar atom; ions with higher internal energy dissociate the Ar atom before photodissociation. Geometries and vibrational frequencies of the Ar attached ions, $Al^+(CH_3OH)_3$-Ar, were then calculated for **3-I(2+1)**. In Fig. 6, the Ar atom binding sites are shown by gray arrows. Vibrational frequencies of the free OH stretching in **3-I(2+1)a** and **3-I(2+1)b** were calculated to be 3605 and 3589 cm^{-1}, respectively, as shown in Table 3. The energy difference between these two vibrations is 16 cm^{-1}, which corresponds to the energy difference between the two peaks, 3615 and 3630 cm^{-1}, observed in the free OH stretching region of the spectrum for $Al^+(CH_3OH)_3$-Ar. From this result, the bands observed at 3615 and 3630 cm^{-1} can be assigned to the free OH stretching vibrations of **3-I(2+1)b** and **3-I(2+1)a**, respectively. Therefore, the third methanol molecule should bind with other methanol molecules solvating to Al^+, without forming a direct bond with the metal ion.

For the n=4 ion, only a spectrum of a nascent $Al^+(CH_3OH)_4$ ion could be measured because the intensity of an $Al^+(CH_3OH)_4$-Ar ion was too small to be observed as photofragment ions. Optimized structures and vibrational spectra of the $Al^+(CH_3OH)_4$ ion are shown in Figs. 8 and 9, respectively. Geometry optimization of the n=4 ion was performed only for the solvated-type isomers because observed features in the spectrum can be well reproduced by the solvated types as noted below, and also because the characteristic band at above 3700 cm^{-1} for the CO-inserted types was hardly observed in the spectrum. We also ruled out the OH-inserted types because it was expected to be less stable than the CO-inserted types by analogy with the results on n=1-3. Four isomers of the $Al^+(CH_3OH)_4$ ion were calculated as equilibrium structures, all of which were classified as solvated type

isomers as shown in Fig. 8. Isomers **4-I(3+1)** and **4-I(3+1)'** have an ion core of **3-I(3+0)**, in which the fourth methanol binds to the methanol molecule(s) of **3-I(3+0)** with one or two hydrogen bonds. On the other hand, **4-I(2+1+1)** and **4-I(2+2)** have the same geometry of ion cores with **3-I(2+1)** and **2-I**, respectively. The fourth methanol molecule in **4-I(2+1+1)** forms a hydrogen bond with a methanol in the second solvation layer of **3-I(2+1)** whereas **4-I(2+2)** has a ring structure of four methanol molecules and the Al^+ ion. Among these solvated type isomers, **4-I(2+1+1)** was found to be the most stable structure as shown in Fig. 8. In the vibrational spectra of these isomers shown in Fig. 9, the spectrum of **4-I(2+1+1)** [Fig. 9(d)] shows good agreement with the experimental spectrum, although relative intensity of the observed spectrum is somewhat different from the calculated one. Thus, **4-I(2+1+1)** was concluded to be predominant in the cluster ion beam.

C. Insertion Reaction

The insertion reaction, which was reported already for the $Al^+(H_2O)_n$ ion by Inokuchi et al.,[11] is discussed in this section. As noted in the introduction, stability of isomer determines whether the insertion reaction occurs or not in the $Al^+(H_2O)_n$ system. However, the most stable isomer, **1-III**, was not found to be produced for the $Al^+(CH_3OH)_1$ ion in the present study. In addition, inserted isomers, **2-II** and **2-III**, were hardly produced in this measurement for n=2, in which the least stable solvated isomer **2-I** was found to be predominant. This feature is the same for the n=3 ion; less stable, solvated type isomer was predominantly formed. These results suggest that the potential energy barriers between inserted type isomers and the solvated isomers are more important than the stability of isomers. Potential energy barriers between **1-I** and **1-II**, and between **1-I** and **1-III** were then calculated at B3LYP/6-31+G(d) level of theory. Figure 10 shows energy diagram of the $Al^+(CH_3OH)_1$ system including predicted geometries of the transition states, TSs, for the

insertion reactions. For the insertion reaction into the OH bond, the potential energy barrier was calculated to be 2.35 eV. This value is larger than the binding energy of the Al^+ ion and the methanol molecule in **1-I**, 1.44 eV. Therefore, it is difficult to form **1-II** from the reaction between Al^+ and CH_3OH. The insertion reaction to form **1-III** was found to proceed with at least two steps; a rotation of a methyl group is necessary to form **1-III** from **1-I** in addition to the insertion reaction of the Al^+ ion into the CO bond, although these two steps, TS2 and TS2', could not be connected directly as shown by a dotted line in the figure. As shown in Fig. 10, there is an energy barrier of at least 1.81 eV for the reaction. This value is also larger than the binding energy between Al^+ and a methanol as noted above. Therefore, the inserted type isomers, **1-II** and **1-III**, were not produced in the present cluster source because of the high reaction barriers. Although there is no information on the potential barriers for the $n \geq 2$ ions and also for the $Al^+(H_2O)_n$ ions at present, one possible explanation of the difference between the methanol and water systems is that the barriers of $Al^+(CH_3OH)_n$ is larger than that of $Al^+(H_2O)_n$ and thus $Al^+(CH_3OH)_n$ ions cannot overcome the potential energy barriers to form the inserted type isomers.

6. Conclusion

Infrared photodissociation spectra of cluster ions containing an Al^+ ion and methanol molecules, $Al^+(CH_3OH)_n$ (n=1-4), have been measured to examine the solvation structures and a possibility of intracluster reactions. In addition, spectra of an Ar-attached cluster ions, $Al^+(CH_3OH)_n$-Ar (n=1-3), have been measured in order to get detailed information and also to enhance the dissociation probability. In the spectra of n=1 and 2 ions, sharp absorption bands were observed in the range of 3500-3600 cm^{-1}. The experimentally obtained spectra were found to be well reproduced by the spectra calculated for clusters classified in solvated type isomers with no hydrogen bond. Thus, it is concluded that the methanol molecules

directly coordinate with the Al^+ ion for n=1 and 2. On the other hand, broad and intense bands were observed in the region of 3000-3500 cm^{-1} for n=3 and 4, in addition to sharp peaks of free OH stretching vibrations. These red-shifted bands show the existence of hydrogen bonds in the clusters. Thus, the third and fourth methanol molecules do not have direct bond with Al^+ but have hydrogen bonds with methanol molecules in the first solvation layer. From the consideration based on the results of theoretical calculations, it was found that the third methanol molecule has two hydrogen bonds with the first and second methanol molecules in n=3, and that the fourth methanol molecule binds with the third methanol in n=4. Furthermore, the intracluster insertion reaction reported in the $Al^+(H_2O)_n$ system was discussed from the potential energy barriers as well as the stability of cluster ions. In the $Al^+(CH_3OH)_n$ cluster ions, no evidence of the insertion reaction was obtained in the present study, although the inserted type isomers were calculated to be more stable than the solvated type isomers at n=1-3. The potential energy barriers to lead inserted type isomers were calculated to be 1.8-2.4 eV for n=1. One possible explanation of the difference between the methanol and water systems is that the barriers in the $Al^+(CH_3OH)_n$ system is larger than that in $Al^+(H_2O)_n$. Therefore, $Al^+(CH_3OH)_n$ ions cannot overcome the potential energy barriers to form the inserted type isomers, although neither information on the potential barriers are available for $n\geq2$ ions nor for the $Al^+(H_2O)_n$ ions at present.

Acknowledgement

This work was supported by the Joint Studies Program (2004) of the Institute for Molecular Science. A part of this work was also supported by "Nanotechnology Support Project" and Grant-in-Aid for Scientific Research of the Ministry of Education, Culture, Sports, Science and Technology (MEXT), Japan. The computations were performed using Research Center for Computational Science, Okazaki, Japan. A. F. is supported by the

Research Fellowship of the Japan Society for the Promotion of Science for Young Scientists.

References

(1) Okumura, M.; Yeh, L. I.; Myers, J. D.; Lee, Y. T. *J. Chem. Phys.* **1986**, *85*, 2328.

(2) Chang, H.-C.; Wu, C.-C.; Kuo, J.-L.; *Int. Rev. Phys. Chem.* **2005**, *24*, 553.

(3) Robertson, W. H.; Diken, E. G.; Price, E. A.; Shin, J.-W.; Johnson, M. A. *Science* **2003**, *299*, 1367.

(4) Headrick, J. M.; Diken, E. G.; Walters, R. S.; Hammer, N. I.; R. Christie, A.; Cui, J.; Myshakin, E. M.; Duncan, M. A.; Johnson, M. A.; Jordan, K. D. *Science* **2005**, *308*, 1765.

(5) Miyazaki, M.; Fujii, A.; Ebata, T.; Mikami, N. *Science* **2004**, *304*, 1134.

(6) Fielicke, A.; Kirilyuk, A.; Ratsch, C.; Behler, J.; Scheffler, M.; von Helden, G.; Meijer, G. *Phys. Rev. Lett.* **2004**, *93*, 023401.

(7) Lisy, J. M. *Int. Rev. Phys. Chem.* **1997**, *16*, 267.

(8) Duncan, M. A. *Int. Rev. Phys. Chem.* **2003**, *22*, 407.

(9) Walker, N. R.; Walters, R. S.; Duncan, M. A. *New J. Chem.* **2005**, *29*, 1495.

(10) Walters, R. S.; Jaeger, T. D.; Duncan, M. A. *J. Phys. Chem. A* **2002**, *106*, 10482.

(11) Inokuchi, Y.; Ohshimo, K.; Misaizu, F.; Nishi, N. *Chem. Phys. Lett.* **2004**, *390*, 140.

(12) Watanabe, H.; Iwata, S. *J. Phys. Chem.* **1996**, *100*, 3377.

(13) Mune, Y.; Ohashi, K.; Ino, T.; Inokuchi, Y.; Judai, K.; Nishi, N.; Sekiya, H. *Chem. Phys. Lett.* **2006**, *419*, 201.

(14) Bullert, D; Breckenridge, W. H. *Chem. Rev.* **2002**, *102*, 1595.

(15) Becke, A. D. *J. Chem. Phys.* **1993**, *98*, 5648.

(16) Frisch, M. J.; Trucks, G. W.; Schlegel, H. B.; Scuseria, G. E.; Robb, M. A.; Cheeseman, J. R.; Montgomery, J. A., Jr.; Vreven, T.; Kudin, K. N.; Burant, J. C.; Millam, J. M.; Iyengar, S. S.; Tomasi, J.; Barone, V.; Mennucci, B.; Cossi, M.; Scalmani, G.; Rega, N. Petersson, G. A.; Nakatsuji, H.; Hada, M.; Ehara, M.; Toyota, K.; Fukuda, R.; Hasegawa, J.; Ishida, M.; Nakajima, T.; Honda, Y.; Kitao, O.; Nakai, H.; Klene, M.; Li, X.; Knox, J. E.; Hratchian, H.

P.; Cross, J. B.; Adamo, C.; Jaramillo, J.; Gomperts, R.; Stratmann, R. E.; Yazyev, O.; Austin, A. J.; Cammi, R.; Pomelli, C.; Ochterski, J. W.; Ayala, P. Y.; Morokuma, K.; Voth, G. A.; Salvador, P.; Dannenberg, J. J.; Zakrzewski, V. G.; Dapprich, S.; Daniels, A. D.; Strain, M. C.; Farkas, O.; Malick, D. K.; Rabuck, A. D.; Raghavachari, K.; Foresman, J. B.; Ortiz, J. V.; Cui, Q.; Baboul, A. G.; Clifford, S.; Cioslowski, J.; Stefanov, B. B.; Liu, G.; Liashenko, A.; Piskorz, P.; Komaromi, I.; Martin, R. L.; Fox, D. J.; Keith, T.; Al-Laham, M. A.; Peng, C. Y.; Nanayakkara, A.; Challacombe, M.; Gill, P. M. W.; Johnson, B.; Chen, W.; Wong, M. W.; Gonzalez, C.; Pople, J. A.; *Gaussian 03*, revision C.02; Gaussian, Inc.: Wallingford CT, 2004.

(17) Vaden, T. D.; Weinheimer, C. J.; Lisy, J. M. *J. Chem. Phys.* **2004**, *121*, 3102.

(18) Inokuchi, Y.; Ohshimo, K.; Misaizu, F.; Nishi, N. *J. Phys. Chem. A* **2004**, *108*, 5034.

Figure captions

Fig. 1. Infrared photodissociation spectra of bare $Al^+(CH_3OH)_n$ (n=1-4) (broken lines) and $Al^+(CH_3OH)_n$-Ar (n=1-3) (solid lines) obtained by monitoring $Al^+(CH_3OH)_{n-1}$ and $Al^+(CH_3OH)_n$ ions, respectively, as a function of the frequency of the dissociation infrared light. The intensities of these spectra were normalized at the most intense band peak position.

Fig. 2. Optimized structures of (a)$Al^+(CH_3OH)_1$, solvated (**1-I**), OH-inserted (**1-II**), and CO-inserted (**1-III**) types, and (b)$Al^+(CH_3OH)_2$, solvated (**2-I**), OH-inserted (**2-II**), and CO-inserted (**2-III**) types, calculated at B3LYP/6-31+G(d) level of theory. ΔE_{rel} shows an energy of each isomer in eV relative to the most stable isomer. Natural charges on Al and some H atoms are shown in parentheses. Gray arrows show Ar-atom binding sites, and neighboring notations (**1-Ia**, **1-Ib**, etc.) indicate isomers in which the Ar atom coordinates from the site denoted by the arrow. Broken lines represent a direct bond to Al^+ ion.

Fig. 3. The optimized structure and an electron density distribution of the HOMO of isomer **1-I** calculated at B3LYP/6-31+G(d). The Ar atom binding sites are also shown by arrows.

Fig. 4. (a)Experimental infrared photodissociation spectra of $Al^+(CH_3OH)_1$ with (black line) and without (broken line) an Ar atom and (b)-(f) calculated vibrational spectra of $Al^+(CH_3OH)_1$-Ar at B3LYP/6-31+G(d) level with a scaling factor of 0.9654 for possible isomers.

Fig. 5. (a)Experimental infrared photodissociation spectra of $Al^+(CH_3OH)_2$ with (black line) and without (gray line) an Ar atom and (b)-(d) vibrational spectra of the most stable structures

in each type of isomers for $Al^+(CH_3OH)_2$-Ar calculated at B3LYP/6-31+G(d) level with a scaling factor of 0.9654.

Fig. 6. Optimized structures of $Al^+(CH_3OH)_3$, solvated (**3-I**), OH-inserted (**3-II**), and CO-inserted (**3-III**) types, calculated at B3LYP/6-31+G(d) level of theory. Arabic numbers in the parentheses of the notation indicate numbers of methanol molecules coordinating with the Al^+ ion directly (the first number) and solvating to the other methanol molecules (the second number). ΔE_{rel} shows the energy of each isomer in eV relative to the most stable structure. Natural charges on the Al atom are shown in parentheses. Gray and black broken lines represent a direct bond to an Al^+ ion and hydrogen bond to other methanol molecules, respectively. Gray arrows in **3-I(2+1)** represent Ar atom binding sites for the two isomers.

Fig. 7. (a)Experimental infrared photodissociation spectra of $Al^+(CH_3OH)_3$ with (black line) and without (gray line) an Ar atom and (b)-(h) calculated vibrational spectra of $Al^+(CH_3OH)_3$ at B3LYP/6-31+G(d) level with a scaling factor of 0.9654 for possible isomers.

Fig. 8. Optimized structures of the solvated type isomers for $Al^+(CH_3OH)_4$ calculated at B3LYP/6-31+G(d) level of theory. Arabic numbers in the parentheses of the notation indicate numbers of methanol molecules coordinating with the Al^+ ion directly (the first number) and solvating to the other methanol molecules in the first and second layer (the second and third numbers). ΔE_{rel} shows the energy of each isomer in eV relative to the most stable structure. Natural charges on the Al atom are shown in parentheses. Gray and black broken lines represent a direct bond to an Al^+ ion and hydrogen bond to other methanol molecules, respectively.

Fig. 9. (a)Experimental infrared photodissociation spectra of $Al^+(CH_3OH)_4$ without an Ar atom and (b)-(e) calculated vibrational spectra of $Al^+(CH_3OH)_4$ at B3LYP/6-31+G(d) level with a scaling factor of 0.9654 for possible isomers.

Fig. 10. Potential energy barriers in eV and geometries of TSs between **1-I** and **1-II**, and between **1-I** and **1-III** calculated at B3LYP/6-31+G(d) level.

TABLE 1. Observed frequencies (ν_{obs} / cm^{-1}) of $Al^+(CH_3OH)_n$ (n=1-4) and $Al^+(CH_3OH)_n$-Ar (n=1-3).

n	ν_{obs} / cm^{-1}	
	$Al^+(CH_3OH)_n$	$Al^+(CH_3OH)_n$-Ar
1	3485	3495
		~3550
2	3579	3567
		3593
3	3594	3615
	3654	3630
	3000-3500	~3300
		~3370
4	3663	
	<3200	
	3000-3500	

TABLE 2. Calculated vibrational frequencies (ν_{calc} / cm^{-1}) and of $Al^+(CH_3OH)_n$ and $Al^+(CH_3OH)_n$-Ar (n=1 and 2) ions. IR intensities in a $km \cdot mol^{-1}$ unit are also shown in parentheses.

$Al^+(CH_3OH)_n$		$Al^+(CH_3OH)_n$-Ar	
	Free OH		Free OH
1-I	3544 (118)	**1-Ia**	3543 (118)
		1-Ib	3503 (331)
1-II	-	**1-IIa**	-
1-III	3763 (468)	**1-IIIa**	3767 (394)
		1-IIIb	3693 (969)
2-I	3563 (60), 3564 (78)	**2-Ia**	3564 (62), 3565 (76)
		2-Ib	3540 (208), 3568 (67)
2-II	3559 (166)	**2-IIa**	3561 (163)
		2-IIb	3488 (475)
2-III	3593 (169), 3732 (210)	**2-IIIa**	3595 (166), 3732 (203)
		2-IIIb	3527 (464), 3733 (208)
		2-IIIc	3594 (173), 3710 (406)

TABLE 3. Calculated vibrational frequencies (ν_{calc} / cm^{-1}) and of $Al^+(CH_3OH)_n$ (n=3 and 4) and $Al^+(CH_3OH)_3$-Ar ions. IR intensities in a $km \cdot mol^{-1}$ unit are also shown in parentheses.

	$Al^+(CH_3OH)_n$	
	Free OH	H-bonded OH
3-I(3+0)	3566 (77), 3573 (77), 3579 (64)	-
3-I(2+1)	3607 (75)	3260 (240), 3319 (1220)
3-II(3+0)	3581 (67), 3584 (209)	-
3-II(2+1)	3580 (139)	2088 (2678)
3-III(3+0)	3563 (147), 3613 (125), 3747 (146)	-
3-III(2+1)	3631 (85), 3736 (183)	2632 (2443)
3-III(2+1)'	3604 (152), 3633 (58)	3183 (2045)
3-I(2+1)a	3605 (75)	3259 (242), 3318 (1219)
3-I(2+1)b	3589 (180)	3246 (246), 3307 (1297)
4-I(3+1)	3586 (68), 3588 (97), 3635 (64)	3076 (623), 3085 (669)
4-I(3+1)'	3580 (40), 3614 (68)	3332 (194), 3380 (1055)
4-I(2+1+1)	3638 (61)	3098 (316), 3130 (2319), 3231 (725)
4-I(2+2)	3612 (64)	2829 (1775), 3237 (989), 3498 (439)

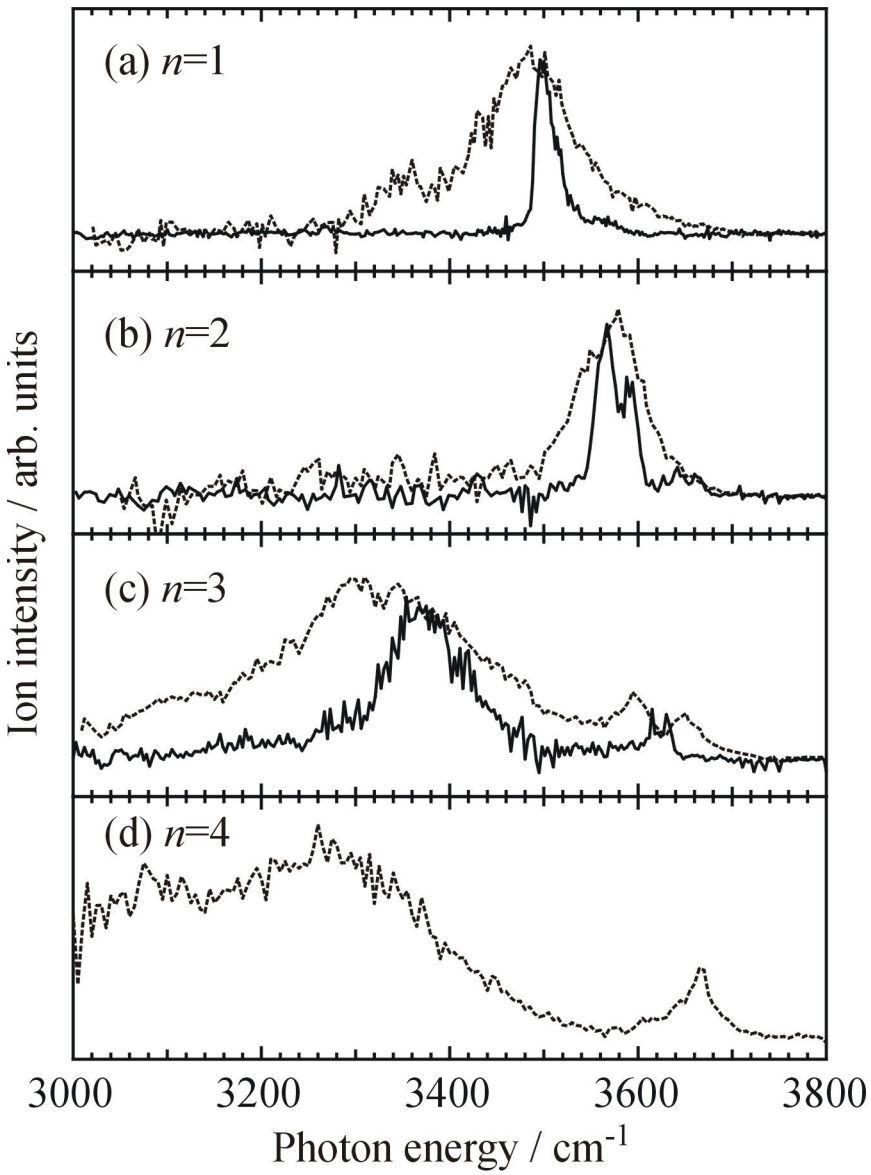

A. Furuya *et al*. Figure 1

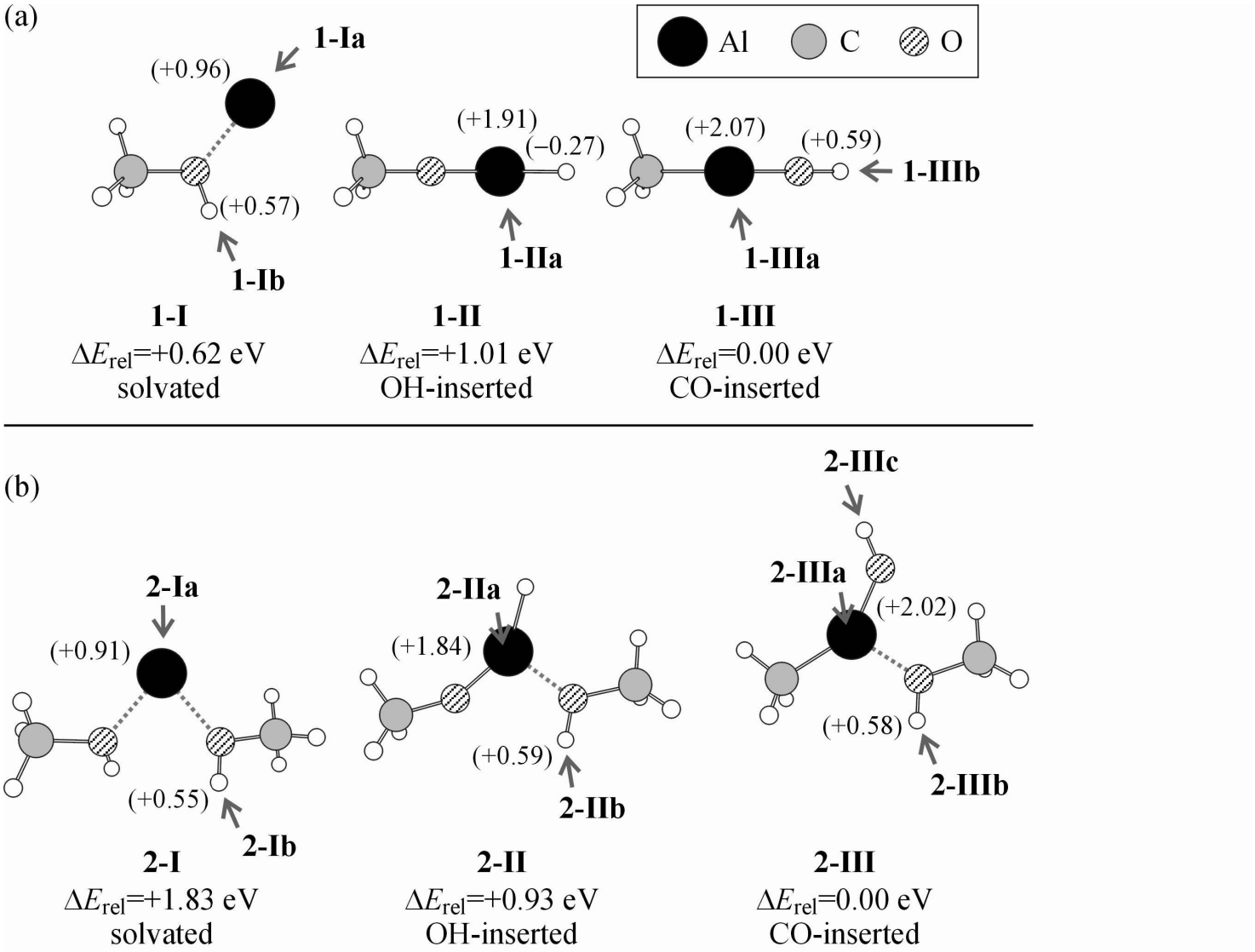

A. Furuya *et al*. Figure 2

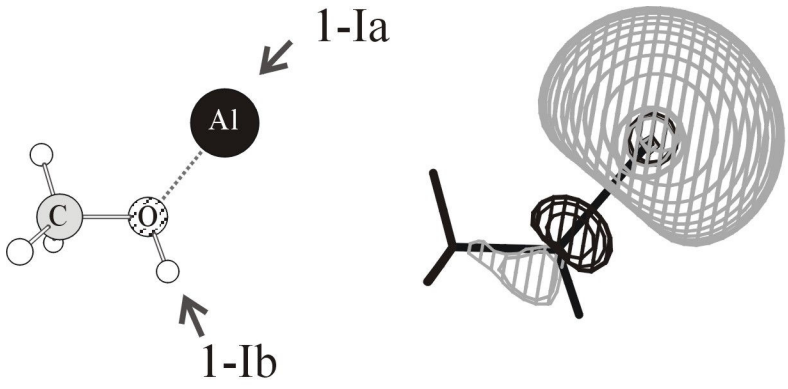

1-I 1-I HOMO

A. Furuya *et al*. Figure 3

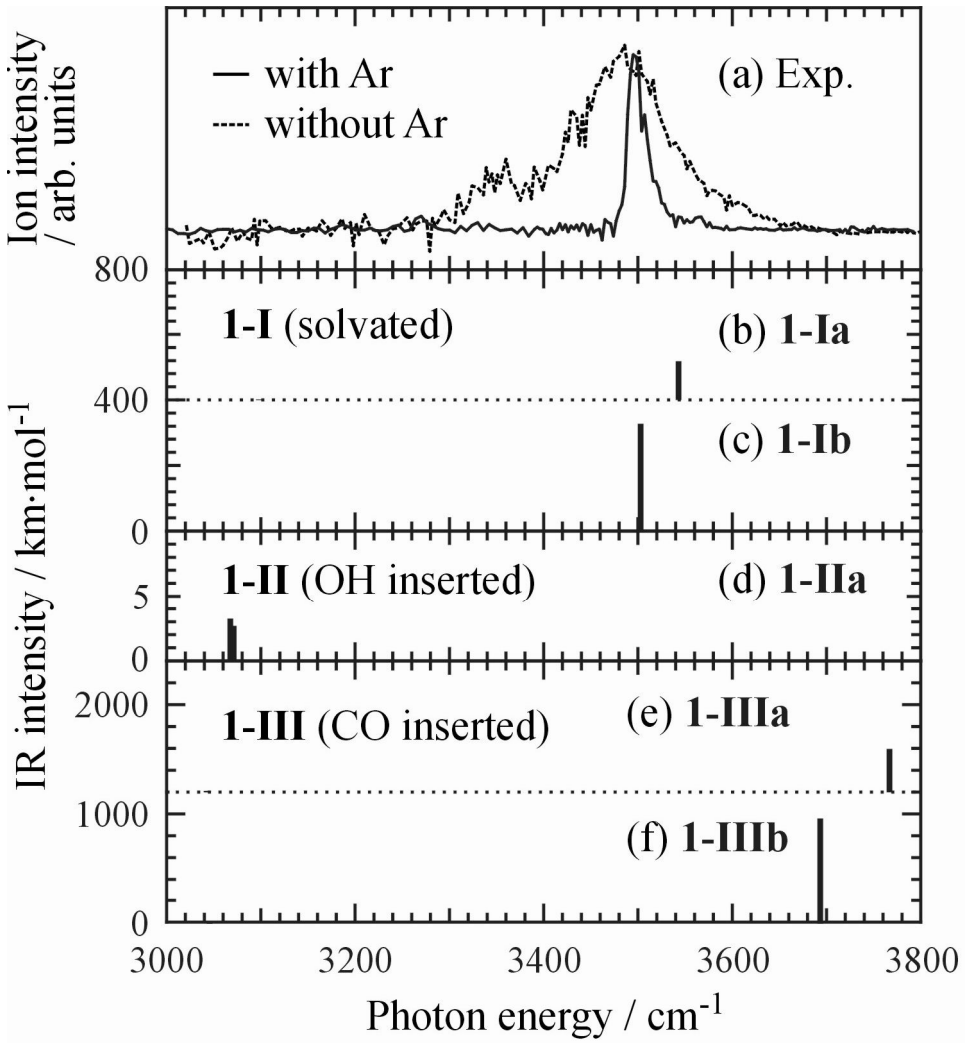

A. Furuya *et al*. Figure 4

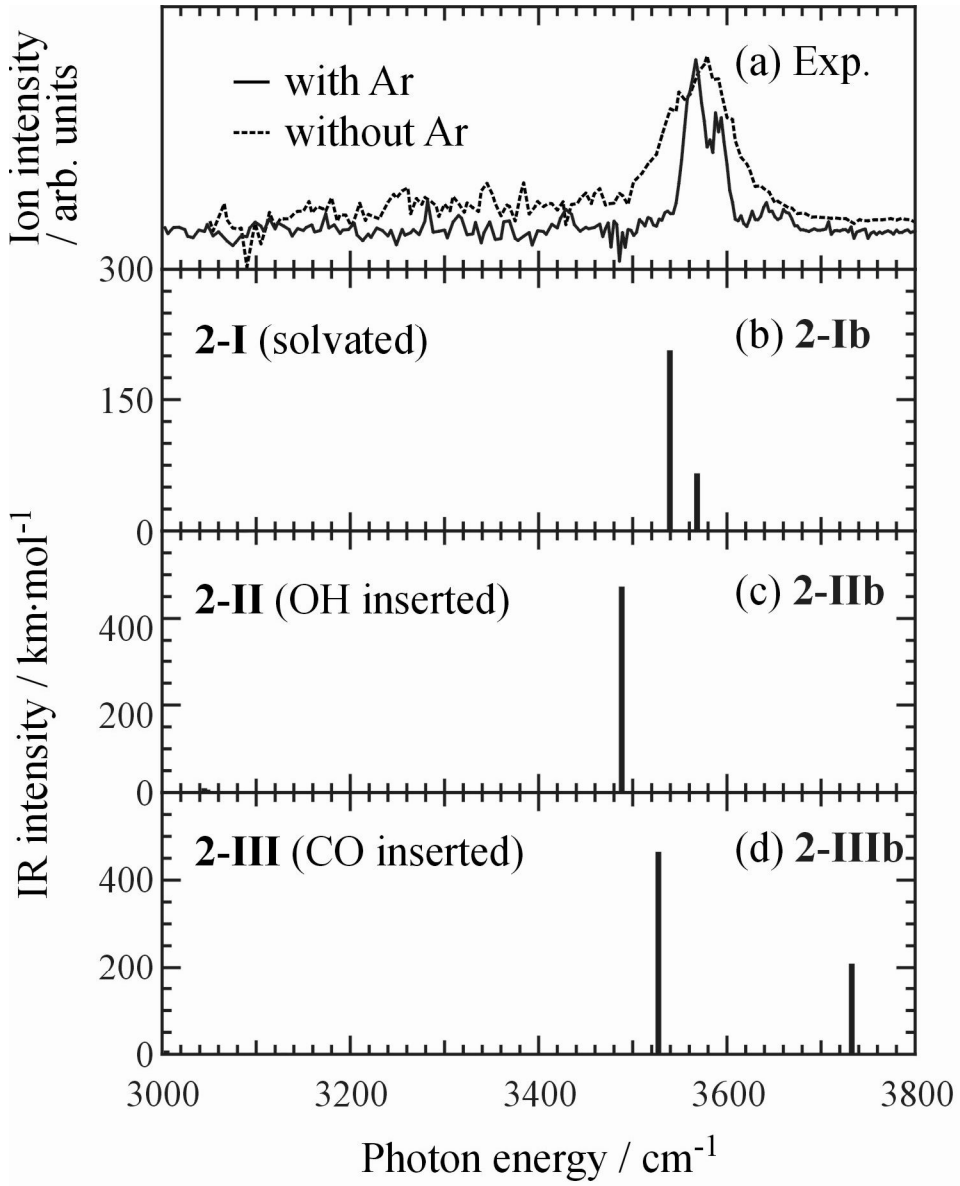

A. Furuya *et al.* Figure 5

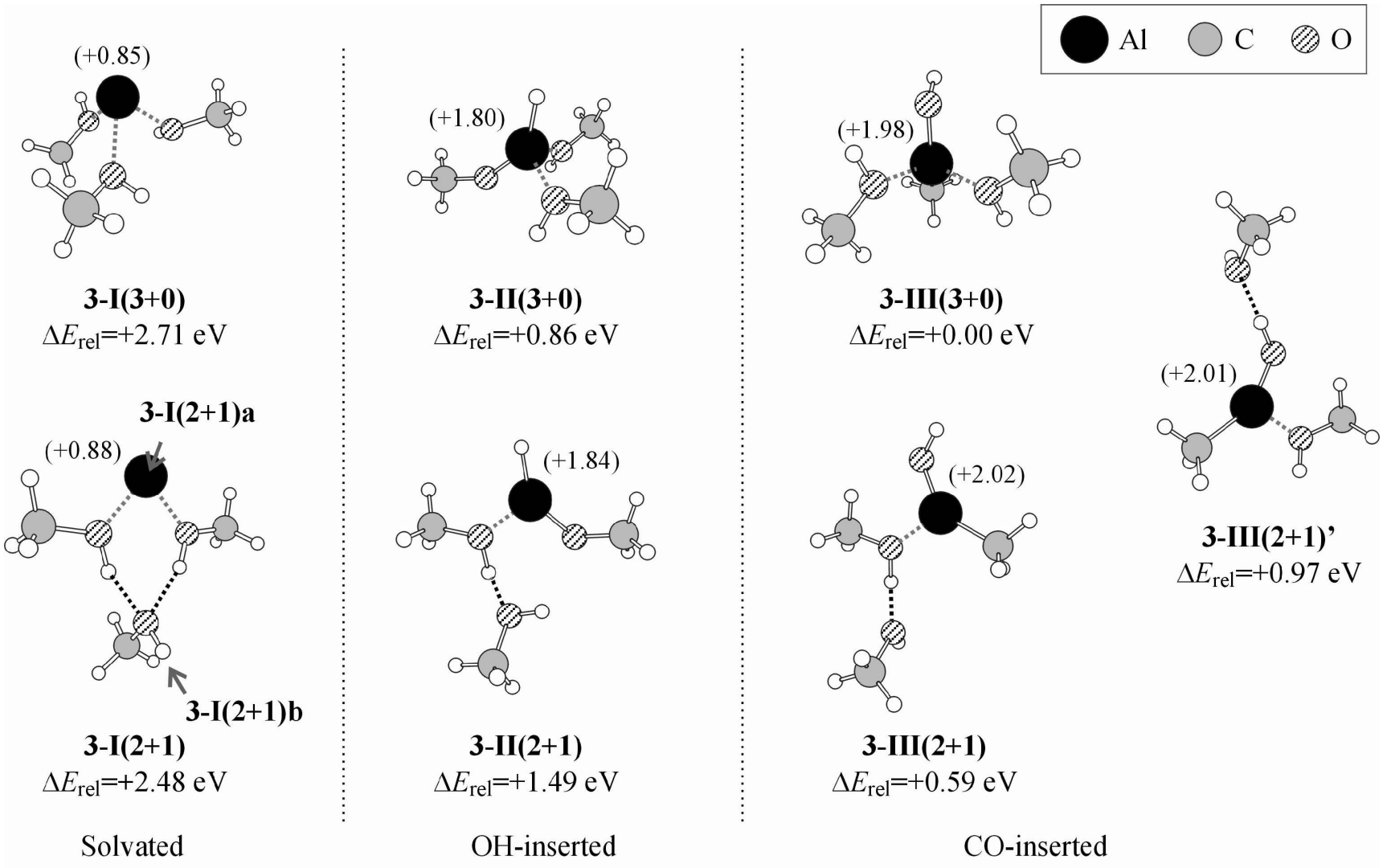

A. Furuya *et al*. Figure 6

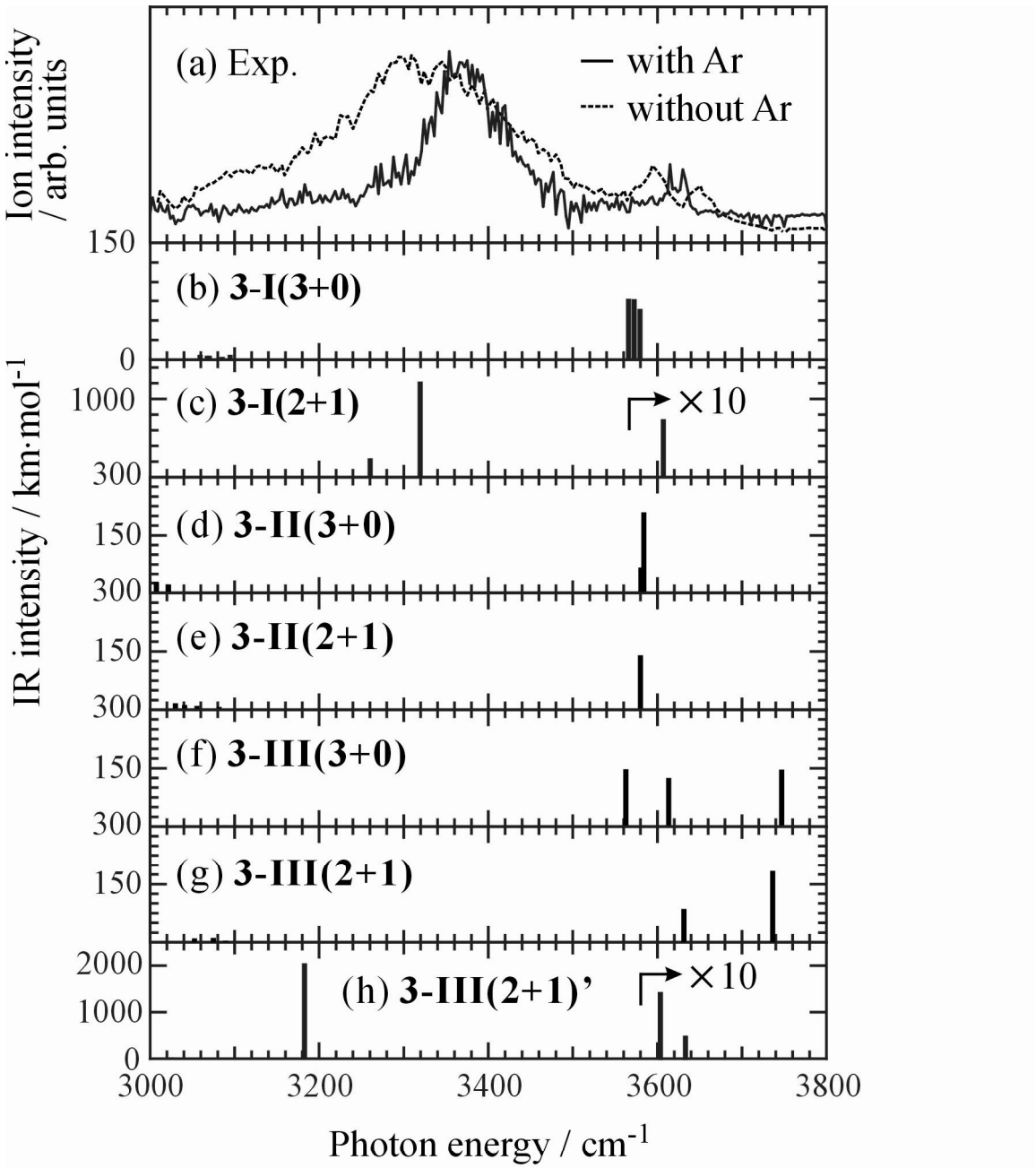

A. Furuya *et al*. Figure 7

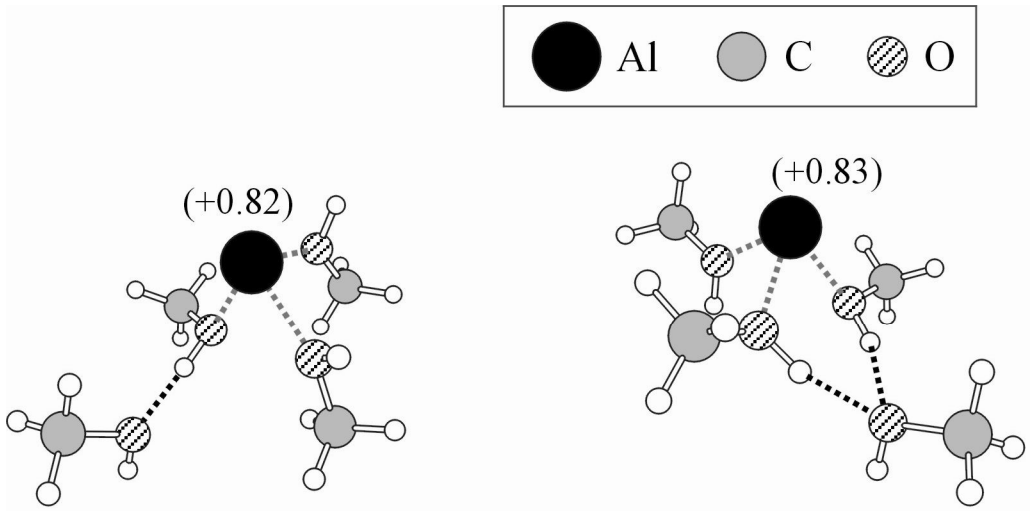

4-I(3+1)
ΔE_{rel}=+0.28 eV

4-I(3+1)'
ΔE_{rel}=+0.14 eV

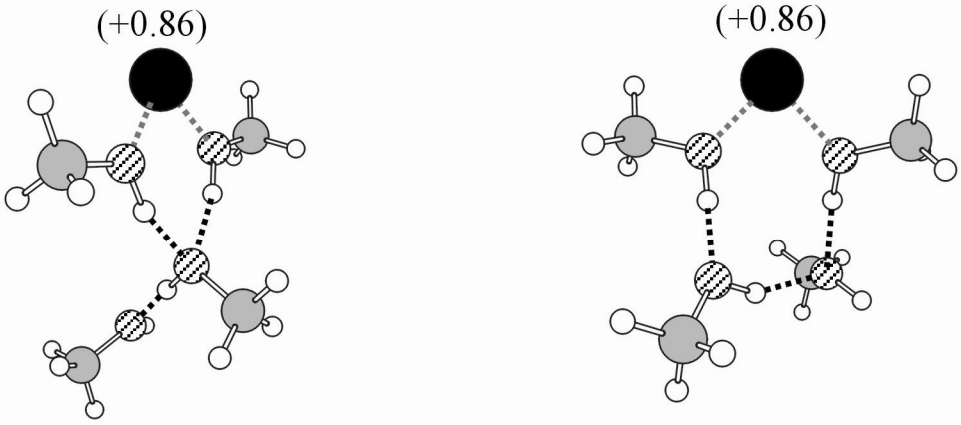

4-I(2+1+1)
ΔE_{rel}=0.00 eV

4-I(2+2)
ΔE_{rel}=+0.10 eV

Solvated

A. Furuya *et al*. Figure 8

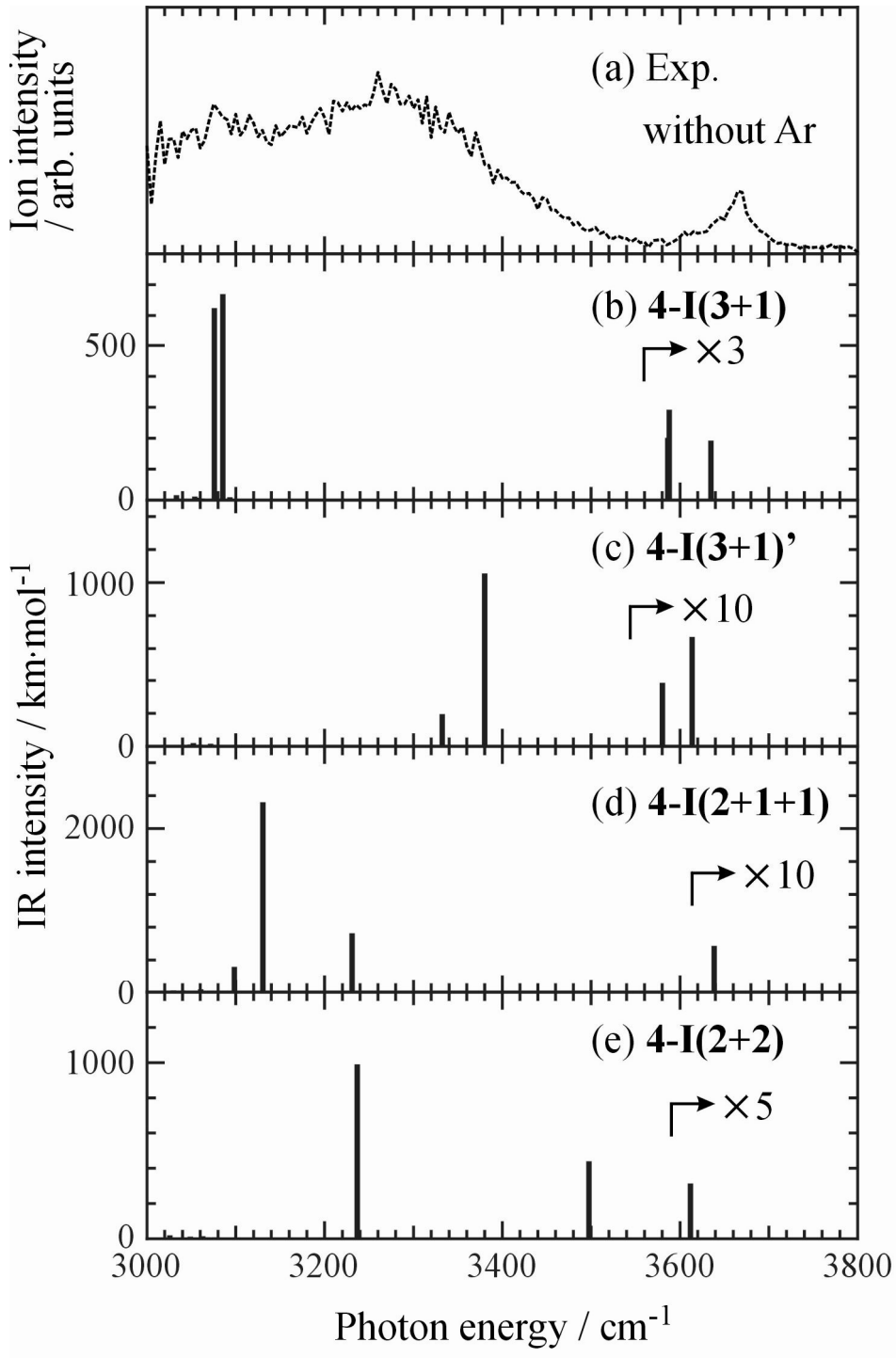

A. Furuya *et al*. Figure 9

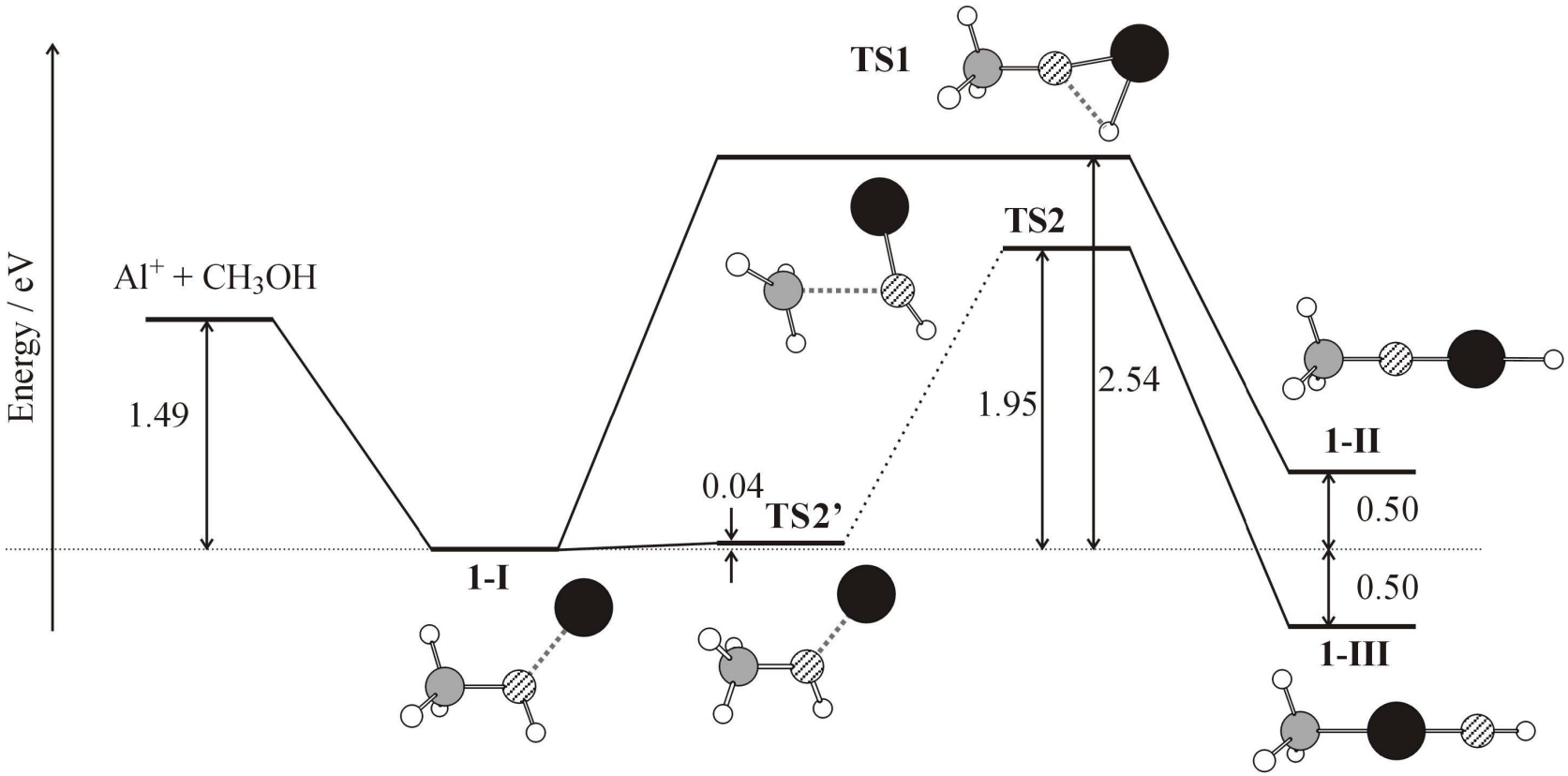

A. Furuya *et al*. Figure 10